Cross-Bridge Number, Position, and Angle in Target Zones of Cryofixed Isometrically Active Insect Flight Muscle

Richard T. Tregear,* Mary C. Reedy,† Yale E. Goldman,‡ Kenneth A. Taylor,§ Hanspeter Winkler,§ Clara Franzini-Armstrong,‡ Hiroyuki Sasaki,¶ Carmen Lucaveche,† and Michael K. Reedy†

*Medical Research Council Laboratory of Molecular Biology, Cambridge CB2 2QH, United Kingdom; †Department of Cell Biology, Duke University Medical Center, Durham, North Carolina 27710 USA; ‡Pennsylvania Muscle Institute, University of Pennsylvania, Philadelphia, Pennsylvania 19194-6083 USA; §Institute of Molecular Biophysics, Florida State University, Florida 32306-4380 USA; ¶Institute of DNA Medicine, Jikei University School of Medicine, 3-25-8 Nishi-shinbashi, Minato-ku, Tokyo 105-8461, Japan

ABSTRACT Electron micrographic tomograms of isometrically active insect flight muscle, freeze substituted after rapid freezing, show binding of single myosin heads at varying angles that is largely restricted to actin target zones every 38.7 nm. To quantify the parameters that govern this pattern, we measured the number and position of attached myosin heads by tracing cross-bridges through the three-dimensional tomogram from their origins on 14.5-nm-spaced shelves along the thick filament to their thin filament attachments in the target zones. The relationship between the probability of cross-bridge formation and axial offset between the shelf and target zone center was well fitted by a Gaussian distribution. One head of each myosin whose origin is close to an actin target zone forms a cross-bridge most of the time. The probability of cross-bridge formation remains high for myosin heads originating within 8 nm axially of the target zone center and is low outside 12 nm. We infer that most target zone cross-bridges are nearly perpendicular to the filaments (60% within 11°). The results suggest that in isometric contraction, most cross-bridges maintain tension near the beginning of their working stroke at angles near perpendicular to the filament axis. Moreover, in the absence of filament sliding, cross-bridges cannot change tilt angle while attached nor reach other target zones while detached, so may cycle repeatedly on and off the same actin target monomer.

INTRODUCTION

Snapshots of active myosin cross-bridges, observed by thin-section electron microscopy (EM) of quick-frozen active muscle fibers, display freeze-trapped structural dynamics of both individual molecules and their ensemble behavior, coupled and constrained in the muscle lattice. Using EM tomography of quick-frozen *Lethocerus* insect flight muscle (IFM), we previously analyzed tilt angles of the myosin motor and light chain binding domains of individual cross-bridges and modeled a hypothetical sequence of structures corresponding to a power stroke of a single motor (Taylor et al., 1999). The binding of these active cross-bridges was restricted to limited segments of the actin filament termed actin target zones.

Actin target zones are defined as contiguous limited segments of the actin helix favorable for myosin attachment. They were first recognized in rigor IFM (Reedy, 1968) and have since been described in detail in rigor and other equilibrium states (Schmitz et al., 1996; Chen et al., 2002). The insect rigor target zones are large; they extend over four actin monomers on each strand of the actin long-pitch helix. Target zones have also been detected in stretch-activated IFM by x-ray diffraction (Tregear et al., 1998) as well as by electron microscopy of fast-frozen IFM during steady-state isometric contraction (Taylor et al., 1999). Binding of myosin heads to actin during active contraction is mostly restricted to smaller target zones of two to three actin monomers along each strand, halfway between successive troponin complexes in each 38.7-nm helical repeat. Target zones have also been described in vertebrate skeletal muscle in rigor (Varriano-Marston et al., 1984; Squire and Harford, 1988; Hirose and Wakabayashi, 1993) and in active vertebrate contraction (Lenart et al., 1996).

The most obvious cause of myosin attachment to limited regions on the actin filament is the azimuthal orientation of the monomers along the actin helix relative to the thick filament (Reedy, 1968). Haselgrove and Reedy (1984) argued that target labeling in IFM rigor muscle simply shows where sterically optimal monomers of the actin helix are presented to an adjacent myosin. Helical selection of actin monomers is not restricted to muscle, nor does it require the presence of the tropomyosin-troponin system. Target zones appear in vitro during active single-molecule interaction between pure actin and myosins II (Molloy et al., 1995), V (Rief et al., 2000; Walker et al., 2000; Veigel et al., 2002), and VI (Rock et al., 2001; Nishikawa et al., 2002). Steffen et al. (2001) reported that the target zone for myosin II in vitro is about three actin monomers long, similar to that seen in active muscle, and appears to be determined by the azimuthal twist of the long-pitch actin helix. In muscle, selective exposure of actin monomers during calcium activation is another possible factor that could modulate axial position and length of actin target zones. In IFM, the large troponin-tropomyosin ensemble is coperiodic with the actin helix (Reedy et al., 1994), and thus could provide differential blocking of actin monomers at each turn of the

Submitted August 19, 2003, and accepted for publication January 6, 2004.

Address reprint requests to Dr. Richard Tregear, Structural Studies Division, MRC Laboratory of Molecular Biology, Hills Rd., Cambridge CB2 2QH, UK. Tel.: 44-1223-365963; Fax: 44-1223-213556; E-mail: rt1@mrc-lmb.cam.ac.uk.

0006-3495/04/05/3009/11 $2.00

helix. Selective exposure could arise from axial variation of actin masking by tropomyosin position under the control of troponin (Narita et al., 2001), possibly mediated by the segmented design of tropomyosin (Brown et al., 2001).

Isometrically activated, tension-generating IFM cross-bridges show a wide range of attachment angles, from prestroke to rigor-like end stroke (Taylor et al., 1999). The range of angles observed in electron micrographic tomograms of rapidly frozen muscle fibers was ordered into a sequence compatible with a continuously attached, progressive 13-nm power stroke. However, the frequency and distribution of cross-bridge positions and angles within the full range were not determined. A range of actomyosin attachment angles has been seen both in isometrically activated vertebrate muscle (Hirose et al., 1993; 1994) and in isolated acto-S1 immediately upon association (Walker et al., 1999). In isometrically active frog muscle, the behavior of the 14.5-nm meridional x-ray reflection is best modeled with cross-bridges nearly perpendicular to the filaments (Dobbie et al., 1998; Irving et al., 2000). In this article we return to the tomograms of isometrically active IFM to quantify the distribution and orientation of attached cross-bridges during isometric contractions. The results suggest that when the filaments cannot slide, the variably angled cross-bridge attachments become locally stabilized in each target zone and that individual tension-generating cross-bridges cycle with little change in axial translocation or angle.

METHODS

Material

The experiments on which this analysis is based were performed on single glycerol-extracted *Lethocerus* dorsal longitudinal muscle fibers activated by raising the free calcium concentration to pCa 4.5 in the presence of Mg·ATP. Briefly, the fibers were slam frozen 10–30 s after isometric tension generation was initiated, then freeze substituted in acetone using a tannic acid-uranyl acetate sequence, and finally embedded in Araldite for thin-section electron microscopy. Three-dimensional (3D) tomograms were calculated from electron micrographic tilt series of regions where longitudinal thin sections contained single myosin and actin filament (MYAC) layers. Each tomogram was computationally flattened and filament straightened (Winkler and Taylor, 1996) to produce a ''raw'' tomogram for analysis of cross-bridge distribution (see Supplementary Material for one example). Raw tomograms were averaged one-dimensionally along the filament axis using the long 116-nm axial repeat (see below). This produced ''column-averaged'' images of improved signal/noise with no lateral averaging between adjacent filaments; these images were used to estimate the axial offsets between myosin shelves on the thick filaments and the centers of target zones on the thin filaments. Successful imaging of thin filament subunit structure in averaged reconstructions of IFM was reported only recently, in rigor muscle using correspondence analysis (Liu et al., 2004), and has not yet been achieved in the active muscle or by the column-averaging method available for our work here. Therefore, we inferred the position of unresolved actin monomers in our analysis of myosin-actin contact variations based on the x-ray diffraction model of IFM actin helices (Miller and Tregear, 1972). Distributions of cross-bridge positions, described later, were determined from unaveraged tomograms. For further details of specimen preparation and image processing, see Taylor et al. (1999).

Observation of cross-bridge images in the raw tomogram

Two of the raw, unaveraged tomograms containing large, continuous, flat, and clear MYAC layer regions were selected for visual tracing of individual cross-bridges attached to actin target zones. These areas extended axially over 9–11 target zones along each thin filament and laterally over 12–15 thin filaments (Fig. 1 *A*). Each tomogram was imported into the model-fitting program IMOD (Kremer et al., 1996) and the (x, y) positions of the actin target zones marked by cross-bridges were mapped to a resolution of 1 pixel (~2 nm). The coordinates used were: x = transverse position across the filament lattice in the plane of the section; y = longitudinal position in the plane of section (M-ward positive); z = transverse position perpendicular to the plane of the section. Each target zone was separately scored for the presence or absence of cross-bridges and for any evident direction of axial tilt from target zone toward thick filament origin, either rigorwards, or antirigorwards. A cross-bridge was only scored when its density could be

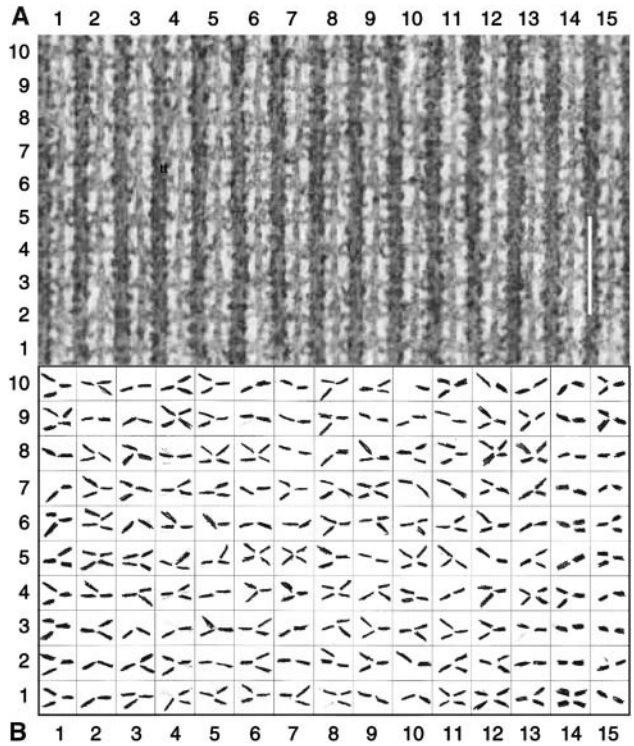

FIGURE 1 Cross-bridge tracing from the raw tomogram. (*A*) Projection of a raw tomogram from a longitudinal section of Ca^{2+}-activated *Lethocerus* flight muscle ($z = \pm 10$ nm relative to the midline of the filaments; see supplementary material for the individual tomogram layers from which this summation was made). The M-line is above and the Z-line is below the overlap zone shown in the image. Cross-bridges at various angles are seen between the thick and thin filaments binding in the actin target zones at 38.7-nm axial intervals on the thin filaments. Some cross-bridges are also seen binding in between the target zones. Contrast has been enhanced to clarify the cross-bridge images (with consequent loss of other details). Scale bar = 100 nm. (*B*) Pattern of target zone cross-bridges traced in the 3D tomogram of the same area. Each outlined box represents a target zone; the correlation with the target zones in Fig. 1 *A* is provided by their horizontal and vertical numbering. The cross-bridges are marked by hand; they were scored when density could be followed from thick to thin filament through a complete set of tomogram layers. The axial position of a cross-bridge origin on the thick filament was recorded as M-ward, Z-ward, or opposite to the visually estimated center of the target zone.

traced continuously from its origin on the thick filament to its target zone on the thin filament by scanning through the 2-nm-thick (x, y) layers. The resultant map of connected cross-bridges in the raw tomogram was recorded manually (Fig. 1 *B*).

Axially averaged (column-averaged) 116-nm segments in tomograms

In *Lethocerus* IFM dense transverse shelves every 14.5 nm along thick filaments contain the myosin heads and their origins (AL-Khayat et al., 2003). Actin target zones, paired on opposite sides of each thin filament, are seen as ~39-nm periodic segments where cross-bridges preferentially attach. The axial repeat distances of the thick filament shelves (14.5 nm) and thin filament target zones (38.7 nm) produce a pattern that repeats every 116 nm; there are three actin target zones and eight shelves in each 116-nm repeat ($8 \times 14.5 = 3 \times 38.7 = 116$ nm). In constructing a column-averaged tomogram, all 116-nm repeats along one thick/thin filament column in the tomogram are axially averaged to yield one 116-nm column average. This process combines the variations in 38.7-nm and 14.5-nm axial repeats to produce one 116-nm averaged triplet of cross-bridge ''motifs,'' and preserves all 116-nm-averaged differences in cross-bridge form and filament profile on each side of every thick and thin filament in the averaged region. A projection image was obtained by stacking 11 (x, y) layers of the column-averaged tomogram (Fig. 2), and this projection image was further analyzed using NIH Image, version 1.62 (O'Neill et al., 1989). Each column between neighboring thick and thin filaments presented a unique averaged cross-bridge pattern, because lateral register between like filaments shifted slightly across the filament lattice.

Derivation of the axial positions of the cross-bridge origins and target zone centers

The column average was used to generate an extended lattice matched to the full area of the raw tomogram. Hence we could calculate the expected axial position at each peak of density representing a myosin shelf and each peak of density representing troponin. Single-pixel width axial density scans of the column-averaged tomograms were obtained adjacent to each thick and thin filament (Fig. 3, *A* and *B*). Certain density peaks on these scans were chosen as reference axial positions. These peaks (*bolded labels* in Fig. 3, *B* and *C*) located non-cross-bridge bearing myosin ''shelves'' on each thick filament edge and the troponin beads on the adjacent thin filament. They were chosen as reference peaks to avoid peaks whose mass centers could be biased by angled or off-center cross-bridge projections. Uniform 14.5-nm and 38.7-repeat scales were aligned with these reference peaks. This alignment defined all axial levels of each repeat on either side of each filament. Hence the positions of each myosin shelf (*Sh1*, *Sh2*, etc.) and troponin (*Tn1*, *Tn2*, *Tn3*; Fig. 3 *B*) within each 116-nm repeat were calculated.

The centers of the thin filament target zones (*Ta1*, *Ta2*, *Ta3*; Fig. 3 *B*) were assumed, for the purposes of calculation, to lie exactly midway between successive troponins. The axial distance from the mass center of each myosin shelf to the center of the adjacent target zone, termed the axial offset (Δy_{SH1}) of the myosin shelf, was calculated on this basis ($\Delta y_{SH1} = y_{SH1} - (y_{TN1} + y_{TN2})/2$; Fig. 3 *C*). Axial offset was defined as positive when the myosin shelf lay M-ward of the target zone center (antirigor cross-bridge angles) and negative when it lay Z-ward of the target zone center (near-rigor cross-bridge angles). It should be noted that the exact values of

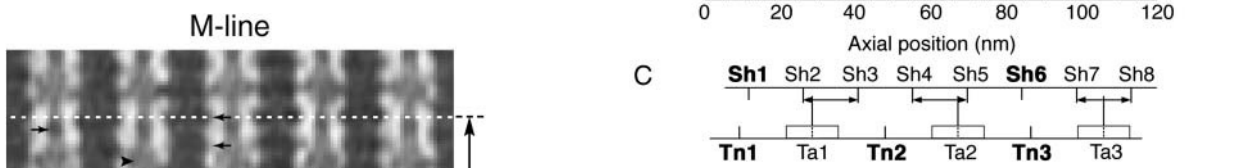

FIGURE 2 The column-averaged tomogram. An axial (116-nm) column average of five of the thin and thick filaments from the tomogram shown in Fig. 1. The 116-nm repeat is shown by horizontal white lines. Note the enhancement of the troponin density (*right-pointing arrows* at 38.7 = 116/3-nm intervals; Reedy et al., 1994), the myosin shelves (*left-pointing arrows* at 14.5 = 116/8-nm intervals), and the target zones (*right-pointing arrowheads*). The cross-bridges are seen as bars connecting the myosin shelves and target zones; the density of a bar in this averaged image is an indication of the frequency with which cross-bridges occur for a particular shelf-target connection.

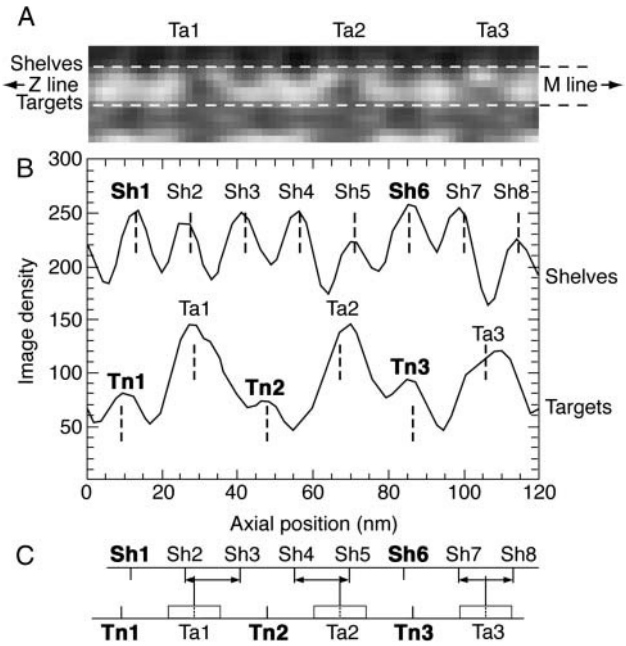

FIGURE 3 The derivation of axial offset between myosin shelf and target zone in a 116-nm column average. (*A*) One example of three actin target zones (*Ta1–Ta3*) and the cross-bridge contacts made to the myosin filament on one side, within the 116-nm repeat from a column-averaged tomogram. The dashed horizontal lines indicate the axial scans from which the density plots shown in *B* were taken. (*B*) Axial scans of density derived from *A*, showing the axial position of myosin shelves on the upper thick filament (*Sh1–Sh8*) relative to actin target zones (*Ta1–Ta3*) and troponins (*Tn1–Tn3*) on the thin filament below. Myosin shelves without target contact are shown bolded. The centers of one troponin bulge and an adjacent myosin shelf that had no cross-bridge density protruding from it (in this case *Tn1* and *Sh1*) were used for alignment of uniform repeat periods of 14.5 nm and 38.7 nm along thick and thin filaments. (*C*) Axial offsets of myosin shelves from actin target zone centers (↔) derived from the uniformly periodic shelf and troponin positions assigned as described in *B*. The target zone centers were placed midway between the troponins. Note that cross-bridges do not bind to the target zone center line but to individual actin monomers within the target zones (cf. Fig. 4 *B*); the approximate extent of the target zones is indicated by the white boxes on the thin filament.

axial offset are particular to each 116-nm-thick thin filament column because the individual filaments were slightly different in axial register.

The axial offset values determined as above were assigned to the corresponding target zones in the raw tomograms by registering the raw and averaged tomograms as follows. First, individual filaments in the raw and column-averaged tomograms were brought into lateral register by direct observation of filament spacing variations. Second, single cross-bridge target zones repeating at three-target intervals were brought into lateral register by aligning a 116-nm triplet of target zone cross-bridges in the clearest column of the raw tomogram with the triplet of cross-bridge motifs in the corresponding column of the column-averaged image. This alignment was checked in other columns, to ensure that a correct overall match had been obtained. By extrapolation from this primary 116-nm match, the 9–11 target zones and the axial offsets for each of the shelves along all thick-thin filament columns in the raw tomograms could be assigned.

Determination of cross-bridge frequency relative to axial offset

The mapped records of cross-bridge presence or absence in each 38.7-nm repeat (Fig. 1 *B*) were noted for each side of each filament and assigned to the axial offsets from the nearest shelves to the given target zone center. Hence, the frequency of cross-bridge occurrence for each column-averaged value of axial offset could be counted by examining each of the shelf-to-target pairings that occurred within the usable area of the tomogram. The data from the individual columns were summed for each tomogram (from 128 target zones in one tomogram and 150 in the other) to obtain the overall frequency of cross-bridge binding related to axial offset at 0.2-nm resolution. To combine the data from the two tomograms without increasing the apparent spread of the data the target zone center positions were adjusted (by +1.2 nm for one tomogram and −0.6 nm for the other), which set the mean axial offset for each tomogram to zero but did not alter the visually apparent near-Gaussian symmetry of the separate plots. The data from both tomograms were then combined and a least-squares procedure was used to find the best-fit Gaussian distribution of cross-bridge frequency versus axial offset.

Displacement of myosin shelves from exactly periodic positions

A separate analysis was used to measure the axial displacement of the cross-bridge-bearing shelf images from their regular 14.5-nm spacing. Two alternative methods of analysis were used to determine the expected zero-strain shelf position to as high an accuracy as possible (0.2 pixels, or 0.4 nm) from the axial density scan close to the thick filament (Fig. 3 *B*). In the first method, a regression line was calculated from the axial positions of the eight shelves in the 116-nm column-averaged unit and the axial displacement of each cross-bridge-bearing shelf from the regression line was determined. In the second method the observed position of each cross-bridge-bearing shelf was subtracted from the calculated position, at uniform 14.5-nm periodic levels between the positions of the two nearest-neighbor cross-bridge-free shelves, and used as a measure of axial displacement. In either method the data were collected according to cross-bridge axial offset, binned in 3.5-nm intervals and a plot of shelf displacement versus axial offset was obtained.

RESULTS

Cross-bridge counts

Electron micrographs and tomograms from calcium-activated isometric *Lethocerus* flight muscle, slam frozen while held isometric at a high tension, show a complex pattern of myosin cross-bridges between thick and thin filaments (Fig. 1 *A*). Although cross-bridge attachment at target zones was visible in all raw tomograms of calcium-activated IFM, reliable scoring of individual cross-bridge connectivity was only feasible within restricted areas (containing 128 and 150 target zones) of two tomograms. Individual cross-bridges were traced through the depth (z) of the 3D tomogram from their origin on the thick filament to their attachment on the thin filament. Many of the cross-bridges appeared narrow along their length, consistent with their being single myosin heads. Fifteen percent (131 out of 851) of the cross-bridges attached to actin outside the 38.7-nm repeated target zones; on average 0.24 cross-bridges were formed on one side of the actin filament in an intertarget region. Half of these intertarget cross-bridges (65/131) were oriented close to perpendicular to the filament array; the rest were equally and widely distributed in the rigor and antirigor directions (Fig. 1 *A*; see also Fig. 3, in Taylor et al., 1999). Half (67/131) of the intertarget cross-bridges were also scored as binding to actin close to the center of the intertarget zone, indicating a greater frequency of attachment in this region than close to the edge of the target zones. Intertarget cross-bridges are infrequent and do not appear to be stereospecific; they are therefore unlikely to contribute greatly to force production. Similar intertarget cross-bridges were observed in tomograms from partial relaxation of IFM by 5′-adenylyl-imidodiphosphate and glycol (Schmitz et al., 1997).

We have concentrated on the 85% (750) of the cross-bridges that bound within actin target zones (Fig. 1 *A*); all numerical data cited below refer to the target zone population alone, without reference to the intertarget zone cross-bridges. A map of the presence or absence of target zone cross-bridges, and their approximate tilt-angle direction, was obtained for each of the two raw tomograms. There were nearly always either one or two cross-bridges scored between each thick and thin filament at a target zone; it was rare to find none formed (two out of 556 cases) and three along one side of the actin filament were never seen (Fig. 1 *B*). The average attachment was ~1.3 cross-bridges/target zone on each side of a thin filament (1.29 and 1.36 in the two tomograms). Where two cross-bridges from one thick filament attached to a thin filament target zone, their origins on the thick filament axially straddled the target zone center (Fig. 1 *B*). In such a cross-bridge pair, the bridge originating M-ward of the target zone center was angled more or less antirigorward (sloping M-wards from the thin filament), whereas the cross-bridge originating closer to the Z-line was angled more or less rigorward (Fig. 1 *B*). We assigned the two cross-bridges to adjacent myosin shelves along the thick filament.

The pattern of axial offset between cross-bridge origin and actin target zone

Column averaging of 116-nm axial segments along each thin filament clarifies regular features and reduces the set of 38.7-

nm repeats along each thick-thin filament interaction column (15–18 in these images) to three different averaged 38.7-nm cross-bridge motifs. Myosin shelves and target zones are enhanced, bars of averaged cross-bridge density are seen connecting them, and the troponin complex can be seen midway between the target zones along the thin filament (Fig. 2). On each side of an actin filament the three averaged target zones typically show a sequence of a near-perpendicular cross-bridge followed by two target zones each bearing cross-bridges from one or both of the flanking shelves above and below.

The column average was used to generate an extended lattice matched to the full area of the raw tomogram. Hence we could calculate the expected axial position at each peak of density representing a myosin shelf (*Sh1–Sh8* in Fig. 3, *A* and *B*) and each peak of density representing troponin (*Tn1–Tn3*). Troponin density set the boundary of the 38.7-nm repeat and the center of the target zone was assigned midway between the troponin densities. The axial distance was estimated between each shelf from which a cross-bridge originated to the center of the target zone in which it attached (Fig. 3 *C*). Axial offset was defined as positive when the myosin shelf lay M-ward of the target zone center and negative when it lay Z-ward of the target zone center. As shelf offset increases M-ward of the target zone, associated bridge angle is increasingly antirigorward. As offset increases Z-ward, associated bridge angle approaches the rigor angle.

The shelves were evenly spaced at 14.5-nm intervals, rendering it possible to look for any deviations of their axial position that might result from holding or generating tension. If subfragment-2 is compliant, strain could cause the positions of the myosin shelves to deviate from their 14.5-nm periodic interval. Because possible deviations were expected to be small, we used two independent methods to assess them (see Methods for details); both methods gave similar results. The data below are derived from comparing cross-bridge-bearing shelf positions to their unstrained positions predicted by linear regression of the whole set of myosin shelves. There was a slight indication that shelves bearing antirigorward cross-bridges were displaced Z-ward (-0.28 ± 0.08 nm (mean $\pm$ SE); $n = 54$), and shelves bearing rigorward cross-bridges were displaced M-ward ($+0.26 \pm 0.14$ nm; $n = 52$). Perpendicular cross-bridges showed negligible displacement (-0.09 ± 0.10 nm; $n = 23$). These results could have been caused by the necessity of measuring the shelf origins slightly away (0.5 pixels = 1 nm) from the filament surface because the observed displacements were in the same direction as the angle of the cross-bridge. Thus the Z-ward tilt of the antirigorward cross-bridges would tend to produce a Z-ward displacement of the cross-bridge origins, and vice versa for the rigorward cross-bridge origins. Note that the measured M-ward displacement of the rigorward cross-bridges is in the opposite direction to that expected from stretching due to tension. On this basis there was no indication of stretching of S2 in either the perpendicular or the rigorward cross-bridges, both of which are expected to bear force. The results appear to exclude tension-generated extensions of S2 greater than three standard errors of the sample mean (0.27 nm).

The relationship of cross-bridge frequency to axial offset

To determine the frequency of cross-bridge formation as a function of offset, each myosin shelf ($\sim$1100 in the two tomograms) was marked as having or not having a cross-bridge, along with its value of axial offset from the nearest actin target zone center. The relationship between the frequency of cross-bridge occurrence and axial offset was binned at 2-nm resolution. Each tomogram showed a sharp and nearly symmetrical reduction in the frequency of cross-bridge formation with increasing axial offset (*upward* and *downward triangles* in Fig. 4 *A*). The combined data could be approximately fitted by a Gaussian curve (*continuous line* in Fig. 4 *A*). However, this fit revealed two non-Gaussian factors. First, close to the center of the graph, the relation between frequency and offset was flattened and saturated at 100%. Cross-bridge frequency as defined in this plot could not exceed 100%, because there was only one myosin molecule within a short azimuthal range at a given axial offset (the other myosins on that shelf being 90° away around the thick filament; Morris et al., 1991; Schmitz et al., 1994). Second, a frequency of cross-bridge attachment higher than that of the fitted Gaussian curve persisted out to 8–10-nm axial offset from the target zone center and then dropped steeply beyond 12 nm to a frequency lower than the Gaussian curve.

Using cross-bridge frequency to infer contacts between individual actin and myosin molecules

Axial offset from the target zone center is not a direct measure of the axial distance between a cross-bridge origin and its actin binding site, because the target actin monomers are distributed about the target zone center (Fig. 4, *B* and *C*). To infer the pattern of actomyosin contact from our observations it is necessary first to estimate the number and position of actin monomers in the target zones.

Both electron microscopy and x-ray diffraction indicate that IFM target zones promote active cross-bridge attachment over a span of 2–3 monomers. Raw tomograms commonly show oppositely angled cross-bridges from adjacent 14.5-nm levels converging toward an interposed target zone (Fig. 1), and column averaging verifies a separation of 5–6 nm between such contacts, consistent with binding to adjacent actin monomers (Taylor et al., 1999). Labeling by active cross-bridges is restricted to target zones within approximately one-third of the actin helix and hence ≤ 3

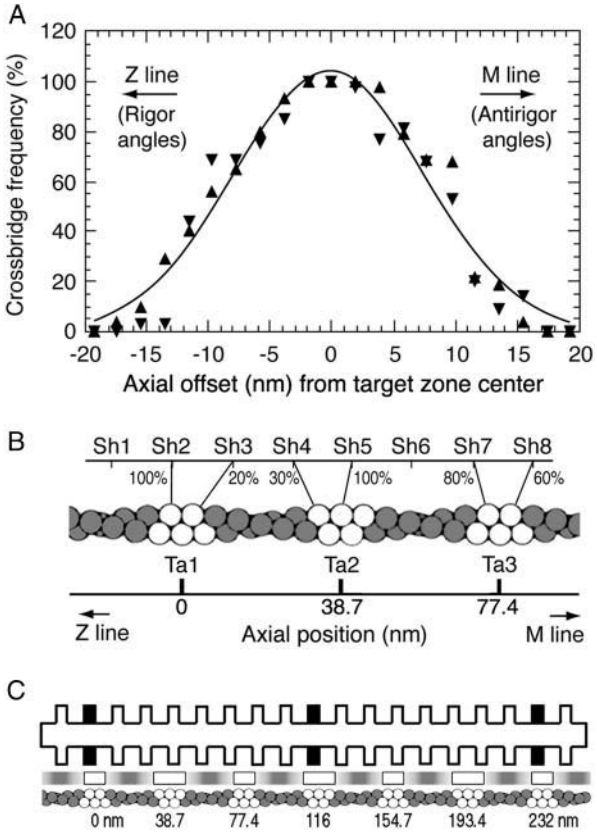

FIGURE 4 Quantitation of cross-bridge attachment. (*A*) The frequency of formation of cross-bridges as a function of the myosin shelf's axial offset relative to the target zone center. The axial offset is considered positive when the shelf is M-ward of target zone so that antirigor cross-bridges would be formed. Observations were made by cross-bridge tracing from 3D raw tomograms (cf. Fig. 1). Data from the two tomograms studied are shown separately (▲; ▼). Each data point was obtained from 27 to 45 observations of the presence or absence of a cross-bridge. Note that the frequency of cross-bridge formation is saturated when the axial offset is <4 nm, remains high up to 8 nm, and is small outside 12 nm. The smooth line is a best-fit unconstrained Gaussian curve ($y = y_{max} \exp(-x^2/2\sigma_x^2)$; $y_{max} = 104\%$; $\sigma_x = 8.0$ nm). (*B*) The position and frequency of cross-bridges attaching to the two- or three-actin monomer-long target zones that are inferred from actin x-ray diffraction in IFM to alternate along one side of a 116-nm length of an actin filament. Sh, myosin shelf origins; Ta, target zone centers. Target zone actin monomers are shown as open circles and intertarget ones as shaded circles. The approximate frequency of interaction (to the nearest 10%) is noted beside each cross-bridge; it was calculated from the data in Fig. 4 *A*. The modeled connections are of nearest-neighbor actin-myosin pairings fitted to alternating two- and three-monomer actin target zones. (*C*) The full unit cell of the actomyosin interaction between two filaments. IFM actin helix structure is known from x-ray diffraction (Miller and Tregear, 1972) and the constant troponin azimuth (Reedy et al., 1993) to repeat exactly, rotating the opposed two- versus three-monomer pattern 180° every 38.7 nm to produce an identical actin target zone repeat every 77.4 nm as shown. The thick filament cross-bridge structure (AL-Khayat et al., 2003) repeats every 116 nm, so that the combined repeats make a unit cell 232-nm long. The frequency of interaction between each shelf and a nearby target zone is indicated by the depth of shading opposite the shelf in the lane between the filaments, with white marking the highest and dark marking the lowest frequency.

actin monomers, according to x-ray diffraction modeling of IFM isometric contraction (Tregear et al., 1998).

The geometry of the thin filament in insect muscle leads to a complication in the modeling of the IFM target zones. In rigor IFM (Miller and Tregear, 1972) the actin forms a helix of 28 subunits in 13 turns. The resulting repeats in the long-pitch two-strand helix at 38.7 nm and 77.4 nm are diagrammed in Fig. 4, *B* and *C*. This geometry leads to an alternating pattern of two-monomer target zones with three-monomer zones on opposite sides of the actin filament at one target level, and an alternation of two with three monomers in successive target zones along one side of the filament. Even though the actin monomers are not individually resolved, this axially successive alternating pattern of three-monomer targets, with the central actin over the target zone center line, and two-monomer targets with the actin pair straddling the target center line (Fig. 4, *B* and *C*), allows us to infer specific actin cross-bridge contacts. Because the two target patterns differ in axial position by a half-monomer spacing, this is our uncertainty limit in modeling shelf-to-monomer distances.

Both our raw tomograms (Fig. 1) and column-averaged tomograms (Taylor et al., 1999) show cross-bridges binding to actin on the same side of the target center as their M-ward or Z-ward shelf origin, so we assume that cross-bridges generally bind to the axially nearest target monomer. Examination of Fig. 4 *B* shows that regardless of the specific value of axial offset measured from shelf to the center line of the target zone, all cross-bridges whose origins sit opposite the two- or three-monomer extent of the target zone are equally well placed to bind actin, because they can be no more than a half-monomer (±2.76 nm) axially displaced from the binding site on one or another target monomer. This measure of proximity holds for myosin origins out to the edge of the outermost target actin monomer (±5.5 nm and 8.3 nm from the target zone center in the alternating two- and three-actin target zones, respectively; Fig. 4 *B*). A large fraction of cross-bridges attach within this range of axial offset (Fig. 4 *A*). Integrating the fitted Gaussian curve, 51% of target cross-bridges lie within ±5.5-nm axial offset of the target zone center, and 69% within ±8.3-nm axial offset of the target zone center. Taking the average frequency for these two offsets, because two-monomer and three-monomer target zones are equal in number, allows us to estimate that the origins of at least 60% of the target cross-bridges lie axially within 2.76 nm of an actin binding site.

The axial displacement between shelf and actin monomer can be used to estimate the overall cross-bridge angle in the MYAC plane. A 2.76-nm axial displacement would produce axial cross-bridge angles within 11° of perpendicular (taking S1 to be 15-nm long). If all cross-bridges originating opposite the target zone were to contact the nearest target actin monomer, they would have axial angles within ±11° of perpendicular to the filaments. If, on the other hand, they tend to bind to the actin monomer closer to the target zone

center, in the three-actin target zone a fraction of these cross-bridges would have tilt angles up to 33°.

For axial offsets beyond the edge of the outermost target monomer (5.5 or 8.3 nm from target zone center), the axial distance between shelf origin and actin increases in parallel with offset, so that the axial angle of the cross-bridge rapidly becomes steeper as offset increases. In this range, the probability of attachment also falls rapidly. Calculating from the Gaussian fit, 17% of the cross-bridges attach from shelves beyond 11.0 nm and 10% from beyond 13.8-nm axial offset. Beyond 11-nm axial offset, cross-bridges bound to two-monomer target zones must reach axially >8.3 nm and hence tilt >33° from the perpendicular, and beyond 13.8 nm this is also true for three-monomer target zones. Our model therefore predicts that 10–17% of target zone cross-bridges tilt >33°. The actual percentage is probably somewhat less because the data points at high axial offset lie below the fitted curve (Fig. 4 *A*).

The lattice array of myosin attachment

The observations described so far have been made in one lattice plane, a MYAC layer, out of the three-dimensional hexagonal array of filaments. Cross-bridge arrangement can also be viewed on a larger scale. The overall pattern of cross-bridge attachment reflects the relative alignment of the helical arrays of myosin and actin molecules within their respective filaments throughout the lattice. The pattern of cross-bridge attachment in IFM depends on the four-start array of myosin origins (S1/S2 junctions) around the myosin shelves relative to the six surrounding actin filaments. Fig. 5 shows a radial projection on a flat surface, viewed from inside the thick filament, of the helical array of myosin origins superimposed on the helical array of actin target zones over a 116-nm repeat (cf. Fig. 4 *B*).

Wray (1979) noted that, at a particular filament overlap, the actin target zones would lie radially opposite the four-start helical tracks of myosin origins on the thick filament, and he suggested that the greatest actomyosin interaction might occur at that matching alignment and provide a structural basis for the strong stretch activation seen in IFM. The particular filament overlap that leads to exactly matched alignment is illustrated in Fig. 5*A* . We have compared our data on active attachment (Fig. 4 *A*) to this helical array. In the matched alignment, those myosin molecules axially close enough to the target zones to bind one head at least two-thirds of the time (according to our data; Fig. 4 *A*) also lie at a small azimuthal angle relative to the target (<20°; *solid bars*, Fig. 5 *A*). The frequency and pattern of attachment developed at this matched alignment appears very consistent with the frequency and pattern of attachment that we observe.

When sliding changes the relative filament overlap by half the repeat period of the actin helix (38.7/2 = 19.35 nm; Fig. 5 *B*), the actomyosin interaction geometry is quite different. A similar set of axial offsets is found, but the axial proximity is no longer correlated with azimuthal proximity. Those myosins within the axial offsets observed to favor cross-bridge formation have to make contact with actin over a large azimuthal range, which would require extreme azimuthal flexibility. This position of filament overlap is therefore less likely to be favored during isometric activation.

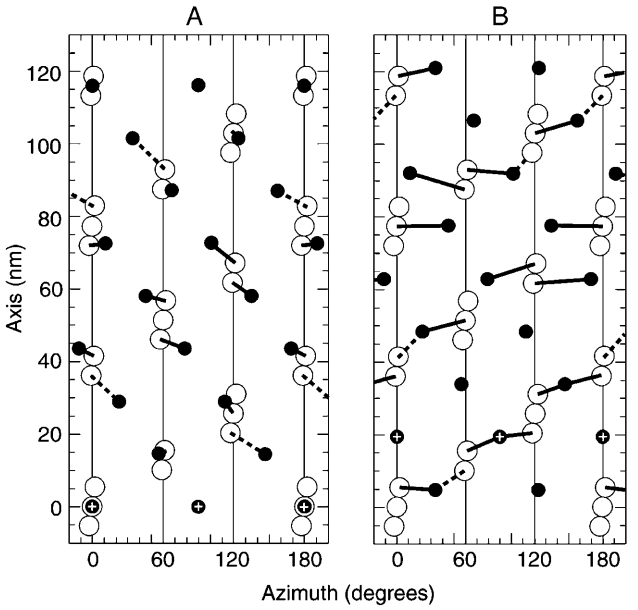

FIGURE 5 Lattice matching of myosin to target zones in isometric contraction. One-half of the cylindrical net diagram of a 116-nm repeat of the thick filament and the interacting thin filaments (Wray, 1979); the pattern repeats in the other half of the cylinder. This diagram is a combined view of the surface of the thick filament and three of the six surrounding thin filaments, in a cylindrical projection as seen from the center of the thick filament. The thin filaments are shown as vertical lines on which the actin monomers of the target zones are drawn as open circles; their slanting angle indicates the direction of the long-pitch actin helix. The thick filament surface array of cross-bridge origins (S1/S2 junctions of myosin heads) is represented by solid circles that form a four-start helix. The black bars are predicted cross-bridges. They are drawn dashed where axial offset is >8 nm (predicted cross-bridge frequency less than two-thirds; Fig. 4 *A*) and omitted wherever either axial offset is >12 nm (predicted cross-bridge frequency less than one-third; Fig. 4 *A*) or azimuthal offset is >50°. (*A*) Relative lattice positions of myosin net and actin target zones in which one origin of a myosin head is exactly over a target zone (*plus-marked solid circles* at base of figure). This aligns the four-stranded RH helix of myosin head origins exactly with the four-stranded RH helix of actin target zones; the web supplement includes a color-coded diagram of these helices. The half cylinder shows 11–15 myosins attached per 116 nm, or 22–30 attached for full cylindrical projection. (*B*) Relative lattice position in which the thick filament is axially displaced by half the 38.7-nm repeat from that shown in *A*. This constitutes an M-ward displacement of the myosin net by 19.3 nm; see plus-marked solid circles. Note the possibility of alternative binding from some cross-bridge origins to either of two thin filament target zones. Construction parameters: a right-handed four-stranded helix of myosin (Reedy et al., 1993; Morris et al., 1991), marked by the S1/S2 junctions of myosin at 14.5-nm axial intervals. The actin filaments are right-handed 28/13, 77.4-nm helices (Miller and Tregear, 1972) arrayed in a 38.7-nm $P6_4$ unit cell (Reedy, 1968).

DISCUSSION

In *Lethocerus* IFM quick frozen during isometric contraction, direct analysis of cross-bridge connection frequency as a function of axial offset from actin target zone center shows that for each myosin molecule facing an actin target zone at the same axial level, one of the two myosin heads binds to actin and is attached nearly all the time. The narrow diameter of cross-bridges seen in active IFM tomograms can typically enclose an atomic model of just one S1 head (Taylor et al., 1999). This is consistent with the x-ray modeling of relaxed insect thick filaments showing that one head of each molecule is much better positioned than the other to bind actin (AL-Khayat et al., 2003). Structural evidence that myosin binds only one of its two heads in the active state is also available from vertebrate muscle, both in situ (Hirose et al., 1994; Juanhuix et al., 2001; Gu et al., 2002) and in vitro (Frado and Craig, 1992; Katayama et al., 1998).

In our tomograms, the binding stoichiometry of myosin (S1) heads is ~1.3 S1/target zone on each side of the thin filament, which represents 36% of the total myosin head content, 3.56 S1/target zone. This percentage is only slightly larger than the estimate derived from x-ray diffraction of similarly activated IFM (29%; Taylor et al., 1999) so the cross-bridges seen in the tomograms probably correspond to a representative sampling of the fully activated isometric IFM. The fraction of myosin heads attached in active frog skeletal muscle estimated by mechanical stiffness is also less than half (43%), once allowance is made for the compliance of the filaments (Linari et al., 1998).

Compared to the 36% of total myosin heads that is actin-bound to actin target zones in these tomograms, the fraction of total actin that is myosin-bound when 1.3 myosin heads attach per 38.7 nm (seven monomers per strand) is less, some 19%. However, the active target zones alternate between two and three actin monomers per side of the filament every 38.7 nm (cf. Fig. 4 *B*). Thus the fraction of target zone actin monomers (2.5 out of seven) occupied by 1.3 myosins per target is much higher, ~50%. It follows that the actin monomers within the target zones are occupied by S1 half of the time (1.3 S1 heads/2.5 actin monomers). In contrast the intertarget actin monomers are only occupied 5% of the time (0.24 cross-bridges/4.5 intertarget actin monomers). In cases where cross-bridges from two myosin shelves interact with a two-actin target zone (e.g., Ta3 in Fig. 4 *B*), both of the target actin monomers are occupied more than half of the time. In such cases, a myosin head newly recharged for force generation with ADP and P_i is likely to find the other target actin monomer occupied so that it, or its partner from the same molecule, will tend to rebind to the same actin monomer at the same cross-bridge angle that preceded its detachment. When the actin target zone consists of three monomers, reattaching myosin heads have more leeway to select alternate actins. The cross-bridges further from target zone centers presumably connect with lower frequency because they spend more of each cycle detached and scanning before settling on the sterically marginal monomers within reach.

Most of the cross-bridges attach from origins directly opposite the actin target zone. According to the deductions made from our results, 60% of the target cross-bridges are formed from myosin shelves opposite to a target actin monomer (taking 2.5 monomers as the average target zone length; see results section for logic). If these cross-bridges attach to the nearest target actin monomer, they will be nearly at right angles to the filaments (within ±11° of the perpendicular to the filament axis). The dominance of near-perpendicular cross-bridges found here is not unique to IFM. Our direct view of this pattern in quick-frozen IFM confirms results from x-ray diffraction of isometrically active frog muscle. Dobbie et al. (1998) and Irving et al. (2000) found that the intensity of the 14.5-nm (M_3) meridional x-ray reflection was nearly maximum in isometric contractions, and was significantly reduced by very rapid cross-bridge responses to sudden releases of small amplitude. Atomic modeling of these myosin head dynamics gave the best fit to the x-ray diagram with an average angle for attached isometric cross-bridges near 90°, from which they are deflected in response to small-length steps.

The total range of origins of target cross-bridges extends to ±11 nm from target zone center and thus ±8.3 nm from the center of the nearest target actin monomer, with resulting tilt angles of as much as 33° away from 90° for a 15-nm long myosin head, but their frequency falls off sharply with increasing offset. Thus relatively few cross-bridges have a large tilt angle. Moreover, there is a symmetric distribution around a near-90° angle. We expected an asymmetric distribution of pre- and end-stroke bridges, with a preponderance from cross-bridge origins shifted toward the Z-line (rigorward angles). In fact, the great majority of the observed cross-bridges are well M-ward of the rigor conformation. Cross-bridges perpendicular to the filaments have their S1-S2 junctions ~6 nm M-ward of the rigor position (Schmitz et al., 1996; Taylor et al., 1999). We find approximately equal numbers of rigorward and antirigorward cross-bridges. This symmetry was unexpected because antirigorward angles favor weakly bound, preforce bridges and rigorward angles favor strongly bound bridges (Holmes, 1997; Goldman, 1998). Whatever specific mechanochemical inferences may be drawn from different cross-bridge angles, the on-off kinetics and force-generating ability would be expected to differ between rigor and antirigor bridges (Geeves et al., 1984; Pate and Cooke, 1989). A kinetic solution to the symmetrical distribution could be that both prestroke and near-rigor bridges are attaching and detaching with similarly rapid kinetics, despite their mechanochemical dissimilarity.

Among the distribution of cross-bridges with different angles, which bear the tension in an isometric contraction? Quick-release experiments on vertebrate and IFM muscle suggest that cross-bridges are capable of generating force

near the isometric level over a range of axial offsets (Huxley and Simmons, 1971; Galler et al., 1996; Reedy et al., 1998). When a contracting muscle is allowed to shorten abruptly by a small amount (a quick release), tension decreases immediately due to the elastic nature of the cross-bridges (the T_1 curve) and then recovers to the isometric value during the next 1–100 ms. For very small quick releases that initiate filament sliding of 5 nm or less, the recovery is nearly complete during the first 1–2 ms, indicating that continuously attached cross-bridges undergo a power stroke to restore tension toward the isometric value (Huxley and Simmons, 1971; Piazzesi et al., 2002). The relationship between the tension after this quick recovery and the amplitude of the rapid length step (the T_2 curve) is quite flat over the range of length steps corresponding to filament sliding of 2-nm antirigorward (stretches) to ~5-nm rigorward (releases). Thus, attached myosin heads produce and maintain high active tension over an ~7-nm range of axial offsets. In combination with the x-ray diffraction data mentioned earlier (Dobbie et al., 1998; Irving et al., 2000), showing the average angle of isometrically active cross-bridges to be near 90°, this ~7-nm range strongly implies that high force is borne in IFM by the 60% of cross-bridges that, originating opposite actin target zones, need span only a 5.5-nm axial offset range (≤2.76-nm offset from nearest target actin monomer). Moreover, the ~7-nm observed range of the flat part of the T_2 curve suggests that some rigorward cross-bridges originating up to 7 nm Z-ward from the target zone center may also bear maximum isometric force.

If the filaments do not slide at all in a truly isometric muscle, the relative positions of myosin shelf and target actin remain unchanged throughout the mechanochemical cycle of an individual cross-bridge. The usual model of the myosin working stroke, in which the lever arm tilts from ~90° to ~45°, would only come into play in an isometric muscle if tilting were permitted by extension of compliance beyond the head-rod junction (e.g., stretch of the S2 portion of myosin rod). However, S2 has been predicted to be quite inextensible (Hvidt et al., 1982; Koubassova and Tsaturyan, 2002) and our observations in this work on the shelf-cross-bridge junction showed no evidence that the head-rod junction is displaced toward the Z-band by tension. It follows that a cross-bridge performs its mechanochemical cycle without axial movement of the head-rod junction relative to the actin and thus without net tilt change in the lever arm. Fluorescence polarization experiments on glycerol-extracted fibers from rabbit muscle, labeled on the regulatory light chain, also showed that tilting of the lever arm is more closely associated with filament sliding than with force generation per se (Irving et al., 1995; Corrie et al., 1999; Hopkins et al., 2002).

Force-generating cross-bridges in isometrically contracting IFM hydrolyze ATP several times per second (Güth et al., 1987), and it is generally assumed that hydrolysis is coupled to a mechanical cycle that passes from zero tension, immediately after ATP binding, to maximum force generation after release of P_i (Goldman, 1987). Force generation with no net lever-arm tilt suggests a flexing cantilever action of the lever arm, similar to the bent fishing pole analogy (with fish hook lodged in an immovable load), as proposed by Goldman (1998), and as explicitly considered by Dobbie et al. (1998) in modeling elastic deformations of the cross-bridge to fit their x-ray results. In isometrically active frog fibers, the elastic deformation of force-generating myosin heads can be completely relieved by an instantaneous (rapid) Z-ward displacement of the head-rod junction relative to actin of ~2.3 nm (Irving et al., 2000). The amount of bending within the lever arm required to accommodate a 2.3-nm displacement is very small and such bending has not yet been reliably demonstrated by electron microscopy. However, suggestive images of internally flexed lever arms of isometric force-generating cross-bridges were previously noted in these tomograms (termed ''V''-shaped cross-bridge in Fig. 4 of Taylor et al., 1999). Whether the cross-bridge needs to release actin in this cycle remains uncertain. Stein et al. (1979; 1981) and White et al. (1997) inferred from the lack of enzymatic inhibition of actomyosin in vitro at high actin concentration and low ionic strength that all the steps of the enzymatic cycle can take place without detachment. Although the experimental material and conditions differed between those studies and ours, the lattice constraints and sterically unchanging presentation of the same target actin monomers to the same cross-bridges in isometrically active fibers could permit a functionally equivalent process in situ. When an actin target zone sits directly opposite a myosin shelf, coupled enzymatic and mechanical cycles could occur repetitively without the S1 detaching from actin. Another possibility is that the two heads of each molecule swap positions on the same actin monomer for each ATP hydrolyzed. In conclusion, our analysis of the cross-bridge pattern observed in isometrically contracting IFM indicates that one of the heads of myosin positioned near actin spends most of its time attached, whereas the other head is unengaged. The geometry of the filament lattice enables this high duty ratio for the active head. The results suggest a view of the cross-bridge cycle in which force generation takes place without significant tilting, unless the filaments slide. Tilting of the lever arm seems to be required to slide the filaments during muscle shortening, but it does not seem to be essential in isometric contraction.

SUPPLEMENTARY MATERIAL

An online supplement to this article can be found by visiting BJ Online at http://www.biophysj.org.

For catching and shipping the live *Lethocerus* waterbugs from which glycerinated IFM was prepared, we thank Torben Poulsen (Heidelberg, Germany and Chiang Mai, Thailand), Gene Scott (Clewiston, FL), and Claudius and Aneta Samuels (Black River, Jamaica).

This work was supported by National Institutes of Health grants GM30598 (Kenneth M. Taylor), HL15835 (Yale E. Goldman and C. Franzini-Armstrong), and AR14317 (Michael K. Reedy).

REFERENCES

AL-Khayat, H. A., L. Hudson, M. K. Reedy, T. C. Irving, and J. M. Squire. 2003. Myosin head configuration in relaxed insect flight muscle: x-ray modeled resting cross-bridges in a pre-powerstroke state are poised for actin binding. *Biophys. J.* 85:1063–1079.

Brown, J.-H., K. H. Kim, G. Jun, N. J. Greenfield, R. Dominguez, N. Volkmann, S. E. Hitchcock-DeGregori, and C. Cohen. 2001. Deciphering the design of the tropomyosin molecule. *Proc. Natl. Acad. Sci. USA.* 98:8496–8501.

Chen, L. F., H. Winkler, M. K. Reedy, M. C. Reedy, and K. A. Taylor. 2002. Molecular modeling of averaged rigor cross-bridges from tomograms of insect flight muscle. *J. Struct. Biol.* 138:92–104.

Corrie, J. E. T., B. D. Brandmeier, R. E. Ferguson, D. R. Trentham, J. Kendrick-Jones, S. C. Hopkins, U. A. van der Heide, Y. E. Goldman, C. Sabido-David, R. E. Dale, S. Criddle, and M. Irving. 1999. Dynamic measurement of myosin light-chain: domain tilt and twist in muscle contraction. *Nature.* 400:425–430.

Dobbie, I., M. Linari, G. Piazzesi, M. Reconditi, N. Koubassova, M. A. Ferenczi, V. Lombardi, and M. Irving. 1998. Elastic bending and active tilting of myosin heads during muscle contraction. *Nature.* 396:383–387.

Frado, L.-L., and R. Craig. 1992. Electron microscopy of the actin-myosin head complex in the presence of ATP. *J. Mol. Biol.* 223:391–397.

Galler, S., K. Hilber, and D. Pette. 1996. Force responses following stepwise length changes of rat skeletal muscle fibre types. *J. Physiol.* 493:219–227.

Geeves, M. A., R. S. Goody, and H. Gutfreund. 1984. Kinetics of acto-S1 interaction as a guide to a model for the crossbridge cycle. *J. Muscle Res. Cell Motil.* 5:351–361.

Goldman, Y. E. 1987. Kinetics of the actomyosin ATPase in muscle fibers. *Annu. Rev. Physiol.* 49:637–654.

Goldman, Y. E. 1998. Wag the tail: structural dynamics of actomyosin. *Cell.* 93:1–4.

Gu, J., S. Xu, and L. C. Yu. 2002. A model of cross-bridge attachment to actin in the A·M·ATP state based on x-ray diffraction from permeabilized rabbit psoas muscle. *Biophys. J.* 82:2123–2133.

Güth, K., K. J. V. Poole, D. Maughan, and H. J. Kuhn. 1987. The apparent rates of crossbridge attachment and detachment estimated from ATPase activity in insect flight muscle. *Biophys. J.* 52:1039–1045.

Haselgrove, J. C., and M. K. Reedy. 1984. Geometrical constraints affecting crossbridge formation in insect flight muscle. *J. Muscle Res. Cell Motil.* 5:3–24.

Hirose, K., and T. Wakabayashi. 1993. Structural change of crossbridges of rabbit skeletal muscle during isometric contraction. *J. Muscle Res. Cell Motil.* 14:432–445.

Hirose, K., T. D. Lenart, J. M. Murray, C. Franzini-Armstrong, and Y. E. Goldman. 1993. Flash and smash: rapid freezing of muscle fibers activated by photolysis of caged ATP. *Biophys. J.* 65:397–408.

Hirose, K., C. Franzini-Armstrong, Y. E. Goldman, and J. M. Murray. 1994. Structural changes in muscle crossbridges accompanying force generation. *J. Cell Biol.* 127:763–778.

Holmes, K. C. 1997. The swinging lever-arm hypothesis of muscle contraction. *Curr. Biol.* 7:R112–R118.

Hopkins, S. C., C. Sabido-David, U. A. van der Heide, R. E. Ferguson, B. D. Brandmeier, R. E. Dale, J. Kendrick-Jones, J. E. T. Corrie, D. R. Trentham, M. Irving, and Y. E. Goldman. 2002. Orientation changes of the myosin light chain domain during filament sliding in active and rigor muscle. *J. Mol. Biol.* 318:1275–1291.

Huxley, A. F., and R. M. Simmons. 1971. Proposed mechanism of force generation in striated muscle. *Nature.* 233:533–538.

Hvidt, S., F. H. Nestler, M. L. Greaser, and J. D. Ferry. 1982. Flexibility of myosin rod determined for dilute solution viscoelastic measurements. *Biochemistry.* 21:4064–4073.

Irving, M., A. T. St-Claire, C. Sabido-David, J. S. Craik, B. Brandmeier, J. Kendrick-Jones, J. E. Corrie, D. R. Trentham, and Y. E. Goldman. 1995. Tilting of the light-chain region of myosin during step length changes and active force generation in skeletal muscle. *Nature.* 375:688–691.

Irving, M., G. Piazzesi, L. Lucii, Y.-B. Sun, J. J. Harford, I. M. Dobbie, M. A. Ferenczi, M. Reconditi, and V. Lombardi. 2000. Conformation of the myosin motor during force generation in skeletal muscle. *Nat. Struct. Biol.* 7:482–485.

Juanhuix, J., J. Bordas, J. Campmany, A. Svensson, M. L. Bassford, and T. Narayanan. 2001. Axial disposition of myosin heads in isometrically contracting muscles. *Biophys. J.* 80:1429–1441.

Katayama, E., G. Ohmori, and N. Baba. 1998. Three-dimensional image analysis of myosin head in function as captured by quick-freeze deep-etch replica electron microscopy. *Adv. Exp. Med. Biol.* 453:37–45.

Koubassova, N. A., and A. K. Tsaturyan. 2002. Direct modeling of x-ray diffraction pattern from skeletal muscle in rigor. *Biophys. J.* 83:1082–1097.

Kremer, J. R., D. N. Mastronarde, and J. R. McIntosh. 1996. Computer visualization of three-dimensional image data using IMOD. *J. Struct. Biol.* 116:71–76.

Lenart, T. D., J. M. Murray, C. Franzini-Armstrong, and Y. E. Goldman. 1996. Structure and periodicities of cross-bridges in relaxation, in rigor, and during contractions initiated by photolysis of caged Ca^{2+}. *Biophys. J.* 71:2289–2306.

Linari, M., I. Dobbie, M. Reconditi, N. Koubassova, M. Irving, G. Piazzesi, and V. Lombardi. 1998. The stiffness of skeletal muscle in isometric contraction and rigor: the fraction of myosin heads bound to actin. *Biophys. J.* 74:2459–2473.

Liu, J., M. C. Reedy, Y. E. Goldman, C. Franzini-Armstrong, H. Sasaki, R. T. Tregear, C. Lucaveche, H. Winkler, B. A. J. Baumann, J. M. Squire, T. C. Irving, M. K. Reedy, and K. A. Taylor. 2004. Electron tomography of fast frozen, stretched rigor fibers reveals elastic distortions in the myosin crossbridges. *J. Struct. Biol.* In press.

Miller, A., and R. T. Tregear. 1972. Structure of insect fibrillar flight muscle in the presence and absence of ATP. *J. Mol. Biol.* 70:85–104.

Molloy, J. E., J. E. Burns, J. C. Sparrow, R. T. Tregear, J. Kendrick-Jones, and D. C. S. White. 1995. Single molecule mechanics of heavy meromyosin and S1 interacting with rabbit or *Drosophila* actins using optical tweezers. *Biophys. J.* 68:298s–350s.

Morris, E. P., J. M. Squire, and G. W. Fuller. 1991. The 4-stranded helical arrangement of myosin heads on insect (*Lethocerus*) flight muscle thick filaments. *J. Struct. Biol.* 107:237–249.

Narita, A., T. Yasunaga, T. Ishikawa, K. Mayanagi, and T. Wakabayashi. 2001. Ca^{2+}-induced switching of troponin and tropomyosin on actin filaments as revealed by electron cryo-microscopy. *J. Mol. Biol.* 308: 241–261.

Nishikawa, S., K. Homma, Y. Komori, M. Iwaki, T. Wazawa, A. H. Iwane, J. Saito, R. Ikebe, E. Katayama, T. Yanagida, and M. Ikebe. 2002. Class VI myosin moves processively along actin filaments backward with large steps. *Biochem. Biophys. Res. Commun.* 290:311–317.

O'Neill, R. R, L. G. Mitchell, C. R. Merril, and W. S. Rasband. 1989. Use of image analysis to quantitate changes in form of mitochondrial DNA after x-irradiation. *Appl. Theor. Electrophor.* 1:163–167.

Pate, E., and R. Cooke. 1989. A model of crossbridge action: the effects of ATP, ADP and P_i. *J. Muscle Res. Cell Motil.* 10:181–196.

Piazzesi, G., M. Reconditi, M. Linari, L. Lucii, Y.-B. Sun, T. Narayanan, P. Boesecke, V. Lombardi, and M. Irving. 2002. Mechanism of force generation by myosin heads in skeletal muscle. *Nature.* 415:659–662.

Reedy, M. K. 1968. Ultrastructure of insect flight muscle. I. Screw sense and structural grouping in the rigor cross-bridge lattice. *J. Mol. Biol.* 31:155–176.

Reedy, M. K., C. Lucaveche, M. C. Reedy, and B. Somasundaram. 1993. Experiments on rigor crossbridge action and filament sliding in insect flight muscle. *Adv. In Exp. Med. and Biology.* 332:33–44.

Reedy, M. C., M. K. Reedy, K. R. Leonard, and B. Bullard. 1994. Gold/Fab immuno electron microscopy localization of troponin H and troponin T in *Lethocerus* flight muscle. *J. Mol. Biol.* 239:52–67.

Reedy, M. K., M. Linari, C. Piperio, and G. Piazzesi. 1998. Tension transients in single fibres from insect flight muscle. *Pflugers Arch.* 436:R20.

Rief, M., R. S. Rock, A. D. Mehta, M. S. Mooseker, R. E. Cheney, and J. A. Spudich. 2000. Myosin-V stepping kinetics: a molecular model for processivity. *Proc. Natl. Acad. Sci. USA.* 97:9482–9486.

Rock, R. S., S. E. Rice, A. L. Wells, T. J. Purcell, J. A. Spudich, and H. L. Sweeney. 2001. Myosin VI is a processive motor with a large step size. *Proc. Natl. Acad. Sci. USA.* 98:13655–13659.

Schmitz, H., C. Lucaveche, M. K. Reedy, and K. A. Taylor. 1994. Oblique section 3-D reconstruction of relaxed insect flight muscle reveals the cross-bridge lattice in helical registration. *Biophys. J.* 67:1620–1633.

Schmitz, H., M. C. Reedy, M. K. Reedy, R. T. Tregear, H. Winkler, and K. A. Taylor. 1996. Electron tomography of insect flight muscle in rigor and AMPPNP at 23°C. *J. Mol. Biol.* 264:279–301.

Schmitz, H., M. C. Reedy, M. K. Reedy, R. T. Tregear, H. Winkler, and K. A. Taylor. 1997. Tomographic 3D reconstruction of insect flight muscle partially relaxed by AMPPNP and ethylene glycol. *J. Cell Biol.* 139: 695–707.

Squire, J. M., and J. J. Harford. 1988. Actin filament organization and myosin head labelling patterns in vertebrate skeletal muscles in the rigor and weak binding states. *J. Muscle Res. Cell Motil.* 9:344–358.

Steffen, W., D. Smith, R. Simmons, and J. Sleep. 2001. Mapping the actin filament with myosin. *Proc. Natl. Acad. Sci. USA.* 98:14949–14954.

Stein, L. A., R. P. Schwartz, Jr., P. B. Chock, and E. Eisenberg. 1979. Mechanism of the actomyosin adenosine triphosphatase. Evidence that adenosine 5′-triphosphate hydrolysis can occur without dissociation of the actomyosin complex. *Biochemistry.* 18:3895–3909.

Stein, L. A., P. B. Chock, and E. Eisenberg. 1981. Mechanism of the actomyosin ATPase: effect of actin on the ATP hydrolysis step. *Proc. Natl. Acad. Sci. USA.* 78:1346–1350.

Taylor, K. A., H. Schmitz, M. C. Reedy, Y. E. Goldman, C. Franzini-Armstrong, H. Sasaki, R. T. Tregear, K. Poole, C. Lucaveche, R. J. Edwards, L. F. Chen, H. Winkler, and M. K. Reedy. 1999. Tomographic 3D reconstruction of quick-frozen, Ca^{2+}-activated contracting insect flight muscle. *Cell.* 99:421–431.

Tregear, R. T., R. J. Edwards, T. C. Irving, K. J. V. Poole, M. C. Reedy, H. Schmitz, E. Towns-Andrews, and M. K. Reedy. 1998. X-ray diffraction indicates that active cross-bridges bind to actin target zones in insect flight muscle. *Biophys. J.* 74:1439–1451.

Varriano-Marston, E., C. Franzini-Armstrong, and J. C. Haselgrove. 1984. The structure and disposition of crossbridges in deep-etched fish muscle. *J. Muscle Res. Cell Motil.* 5:363–386.

Veigel, C., F. Wang, M. L. Bartoo, J. R. Sellers, and J. E. Molloy. 2002. The gated gait of the processive molecular motor, myosin V. *Nat. Cell Biol.* 4:59–65.

Walker, M., X.-Z. Zhang, W. Jiang, J. Trinick, and H. D. White. 1999. Observation of transient disorder during myosin subfragment-1 binding to actin by stopped-flow fluorescence and millisecond time resolution electron cryomicroscopy: evidence that the start of the crossbridge power stroke in muscle has variable geometry. *Proc. Natl. Acad. Sci. USA.* 96:465–470.

Walker, M. L., S. A. Burgess, J. R. Sellers, F. Wang, J. A. Hammer III, J. Trinick, and P. J. Knight. 2000. Two-headed binding of a processive myosin to F-actin. *Nature.* 405:804–807.

White, H. D., B. Belknap, and M. R. Webb. 1997. Kinetics of nucleoside triphosphate cleavage and phosphate release steps by associated rabbit skeletal actomyosin, measured using a novel fluorescent probe for phosphate. *Biochemistry.* 36:11828–11836.

Winkler, H., and K. A. Taylor. 1996. Three-dimensional distortion correction applied to tomographic reconstructions of sectioned crystals. *Ultramicroscopy.* 63:125–132.

Wray, J. S. 1979. Filament geometry and the activation of insect flight muscles. *Nature.* 280:325–326.